A Bidomain Numerical Validation for Assessing Times of Fast and Ending Repolarization from Monophasic Action Potentials

P. Colli Franzone[1], L.F. Pavarino[2], S. Scacchi[1], and B. Taccardi[3]

[1] Dip. di Matematica, Università di Pavia, Via Ferrata 1, 27100 Pavia, Italy
peiro.collifranzone@unipv.it, simone.schacchi@unimi.it
[2] Dip. di Matematica, Università di Milano, Via Saldini 50, 20133 Milano, Italy
luca.pavarino@unimi.it
[3] CVRTI, University of Utah, Salt Lake City, UT 84112, USA
taccardi@cvrti.utah.edu

Summary. 3D numerical simulations of unipolar electrograms (EGs) and hybrid monophasic action potentials (HMAPs) were performed by using the cardiac Bidomain model with homogeneous and heterogeneous Luo–Rudy I membrane models. While estimating local recovery times from EGs can be difficult in case of flat T-waves or linear ST ramps, the HMAP signal always displays a monophasic downstroke as does the transmembrane action potential (TAP) and contains valuable information for assessing repolarization time. The simulation results show that: (a) the HMAP fast repolarization time is a reliable estimate of the TAP fast repolarization time; (b) the HMAP ending (90%) repolarization time is a less reliable estimate of the TAP ending repolarization time; (c) analogous conclusions hold for the associated action potential durations APD and APD90.

1 Introduction

While methods for determining cardiac activation times from electrographic signals recorded directly from the heart have been firmly established, see e.g. [11] and the references therein, there are still uncertainties and controversies about the best method for determining cardiac recovery times. The repolarization time at a given point x of the cardiac domain is related to some time markers associated with the downstroke of the transmembrane action potential (TAP, considered to be the gold standard) recorded at x, or with the T wave of the extracellular unipolar recording (EG) recorded at x. An alternative extracellular technique is based on the downstroke of the hybrid monophasic action potential (HMAP; see [6, 8]) at x, obtained by taking as a reference the potential at a fixed permanently depolarized (PD) site and

A.D. Fitt et al. (eds.), *Progress in Industrial Mathematics at ECMI 2008*,
Mathematics in Industry 15, DOI 10.1007/978-3-642-12110-4_54,

reversing its polarity. The HMAP is equivalent to the difference between the EG at the PD site and the EG at the exploring site x. The HMAP information content during the repolarization phase has been recently questioned and the HMAP genesis has been a controversial subject. In this paper, we present the results of a Bidomain – LR1 3D simulation study showing that HMAPs contains valuable information for assessing both the fast and ending TAP repolarization times, confirming our recent study [4].

2 Methods

2.1 The Bidomain: LR1 Model

Our simulation study is based on the macroscopic bidomain representation of the cardiac tissue coupled with Luo–Rudy I [7] ionic membrane model. This system allows us to compute the intra and extracellular potentials $u_i(x,t), u_e(x,t)$, the transmembrane potential $v(x,t) = u_i(x,t) - u_e(x,t)$, the gating variables $w(x,t)$ and the ionic concentrations $c(x,t)$, as the solutions of the reaction-diffusion system

$$\begin{cases} c_m \dfrac{\partial v}{\partial t} - div(D_i \nabla u_i) + i_{ion}(v,w,c) = -i^i_{app} & \text{in } H \times (0,T) \\ -c_m \dfrac{\partial v}{\partial t} - div(D_e \nabla u_e) - i_{ion}(v,w,c) = i^e_{app} & \text{in } H \times (0,T) \\ \dfrac{\partial w}{\partial t} - R(v,w) = 0, \qquad \dfrac{\partial c}{\partial t} - S(v,w,c) = 0 & \text{on } H \times (0,T) \\ \mathbf{n}^T D_{i,e} \nabla u_{i,e} = 0 & \text{in } \partial H \times (0,T) \\ v(\mathbf{x},0) = v_0(\mathbf{x}), \qquad w(\mathbf{x},0) = w_0(\mathbf{x}), \qquad c(\mathbf{x},0) = c_0(\mathbf{x}) & \text{in } H. \end{cases} \tag{1}$$

Here $c_m = \chi C_m$ and $i_{ion} = \chi I_{ion}$ denote the capacitance and the ionic current of the membrane per unit volume, and $i^{i,e}_{app}$ the applied intra- and extracellular currents per unit volume satisfying the compatibility condition $\int_H i^i_{app} = \int_H i^e_{app}$. χ denotes the surface membrane area per unit volume. The cardiac volume H is considered fully insulated, since we have imposed zero normal fluxes of intra- and extracellular currents. The extracellular potential u_e, defined apart from an independent constant determined by the choice of the reference potential, is determined by the condition $\int_H u_e(x,t)dx = 0$.

2.2 Numerical Methods

The cardiac domain H considered in this study is a cartesian slab of dimensions $1.92 \times 1.92 \times 0.48\,\mathrm{cm}^3$, modeling a portion of the left ventricular wall. In all computations, a structured grid of $192 \cdot 192 \cdot 48$ hexahedral isoparametric Q_1 finite elements of size $h = 0.1\,\mathrm{mm}$ is used in space, while the time discretization is an Implicit-Explicit Euler method. The linear solver at each

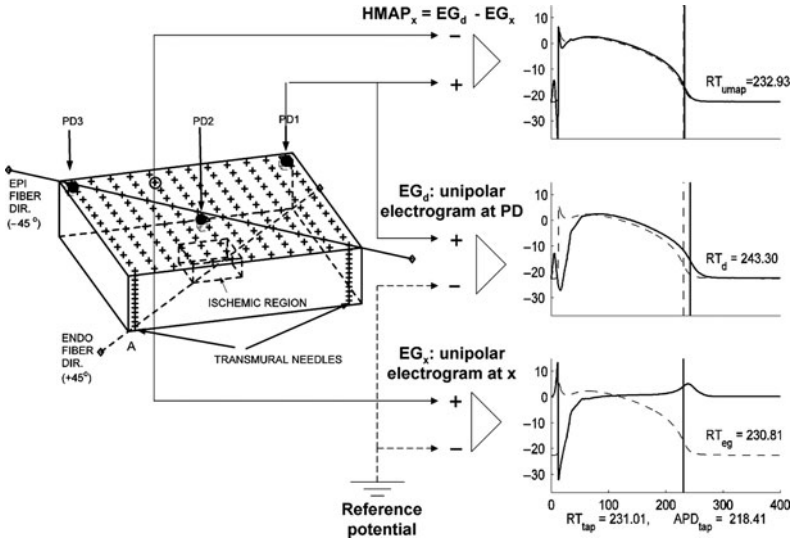

Fig. 1. *Left*: cardiac slab H, permanently depolarized sites PD1, PD2, PD3, ischemic region, transmural needles. *Right*: unipolar electrograms EG_x at the exploring site x (*bottom*) and EG_d at the PD site (*middle*), hybrid monophasic action potential HMAP_x at x (*top*)

time step is the conjugate gradient method, preconditioned by a hybrid multilevel Schwarz preconditioner. We use the PETSc parallel library [1] in order to ensure the parallelization and portability of our code, run on a Linux Cluster with 56 Opteron AMD processors and Infiniband network. Each simulation required about 8 h on 36 processors; further numerical details on our parallel solver can be found in [2,3,9,12].

2.3 Multi-Electrode Array

In our cardiac slab H, we consider a matrix of 12×12 exploring multielectrode needles spaced 1.6 mm from each other and 0.8 mm from the slab boundary, as shown in Fig. 1. Each needle carries 13 recording sites, spaced 0.4 mm along the shank. We then have 12×12 sites on each of the 13 intramural planes, for a total of $12 \times 12 \times 13 = 1{,}872$ recording sites in the slab, each recording the intra and extracellular potentials.

2.4 Potential Waveform and Repolarization Markers

At each recording site x we store the following waveforms:

$\mathrm{EG}_x(t) = u_e(x,t)$: unipolar electrogram at the exploring site x,
$\mathrm{TAP}_x(t) = u_i(x,t) - u_e(x,t)$: transmembrane potential at x,

$\mathrm{HMAP}_x(t) = \mathrm{EG}_d(t) - \mathrm{EG}_x(t)$: hybrid monophasic action potential at x, where $\mathrm{EG}_d(t)$ is the unipolar electrogram at a permanently depolarized site PD (see Fig. 1 and below). From these waveforms, we then compute the following markers of fast repolarization time:

$\mathrm{RT}_{tap}(x)$ = time of min $\partial_t \mathrm{TAP}_x(t)$ during downstroke,

$\mathrm{RT}_{hmap}(x)$ = time of min $\partial_t \mathrm{HMAP}_x(t)$ during downstroke,

and the following markers of ending repolarization time:

$\mathrm{RT90}_{tap}(x)$: instant when $\mathrm{TAP}_x(t) = 90\%$ of its resting value during downstroke,

$\mathrm{RT90}_{hmap}(x)$: instant when $\mathrm{HMAP}_x(t) = 90\%$ of its resting value during downstroke.

2.5 Transmural Heterogeneity

We consider three different types of transmural APD distribution, one homogeneous (H-slab) and the other two heterogeneous (3-slab and W-slab), while in any plane parallel to the epicardium all cells have the same intrinsic APD. In the heterogeneous slabs, the intrinsic APD of the cells is obtained by multiplying the potassium current I_K in the LR1 model by a factor fact_{I_K}, as detailed in Table 1. In this way, we mimic the experimental transmural APD profile with M-cell layers as in [13] (3-slab) or as in [14, Fig. 4], [10, Fig. 5] (W-slab); see [3] for more details.

2.6 Subendocardial Ischemia

Two simulations with subendocardial moderate (MI-slab) and severe (SI-slab) ischemic regions are performed. The ischemic region has dimensions $0.4 \times 0.4 \times 0.16\,\mathrm{cm}^3$ and is located as shown in Fig. 1. In the LR1 model, the current I_K is scaled by a factor 2.325, yielding TAPs with APD90 = 250 ms. Inside the ischemic region, the extracellular potassium concentration $[K]_o$ is increased from 5.4 mM (control) to 10.5 mM (MI-slab) and 18 mM (SI-slab).

Table 1. Parameter calibration for modeling the transmural heterogeneities in the three cardiac slabs H-slab, 3-slab, W-slab

	H-slab	3-slab			W-slab			
# of layers	1	3			4			
		Endo	Mid	Epi	Endo	Sub-endo	Mid	Epi
thickness (cm)	0.48	0.16	0.16	0.16	0.058	0.096	0.254	0.072
fact_I_K	1	2.62	1.95	2.88	2.71	1.95	2.47	2.88
APD (ms)	266	235	272	225	232	272	242	225

2.7 Permanently Depolarized (PD) Volume

In order to generate an almost constant TAP inside a small volume, denoted by permanently depolarized (PD) volume, we assign the extracellular potassium concentration equal to the intracellular one, i.e. I_{K1} is zero in the small PD volume with dimensions $0.8 \times 0.8 \times 0.8\,\mathrm{mm}^3$. We considered three PD sites labeled PD1, PD2, PD3 in Fig. 1, but for brevity we only report the results with PD3.

2.8 Stimulation Site

Inside the PD volume the transmembrane potential values are above threshold thus generating a first excitation-recovery TAP that sweeps the cardiac slab H. We wait for 500 ms and take the steady state reached by the bidomain system as the initial condition for our simulations. An extracellular stimulus ($i^e_{app} = -250\,\mathrm{mA/cm}^3$ for 1 ms) is then applied in a small volume (3 mesh points in each direction) at the locations A in Fig. 1 and an intracellular stimulus $i^i_{app} = i^e_{app}$ is also applied in order to satisfy the compatibility condition for the solvability of the bidomain system 1.

3 Results

The results of Table 2 show a very high correlation coefficient (≥ 0.98) between both the markers of fast repolarization RT_{hmap} and RT_{tap} and the markers of ending repolarization $\mathrm{RT90}_{hmap}$ and $\mathrm{RT90}_{tap}$. This good global matching, confirmed by the regression lines of Fig. 2, top, assures a high reliability of the markers in terms of localizing regions that repolarize first and last and in terms of repolarization patterns. RT_{hmap} provides good estimates of RT_{tap} with average discrepancy of about 2 ms, while $\mathrm{RT90}_{hmap}$ provides less accurate estimates of $\mathrm{RT90}_{tap}$ with average discrepancy of about 4 ms. This lower accuracy is also confirmed by the histograms reported in Fig. 2, bottom.

Table 2. Recovery times and action potential duration markers discrepancies

	RT_{hmap} vs RT_{tap}			$\mathrm{RT90}_{hmap}$ vs $\mathrm{RT90}_{tap}$			ARI_{hmap} vs APD			$\mathrm{ARI90}_{hmap}$ vs APD90		
	Mean	Std	Corr	Mean	Std	Corr	Mean	Std	Corr	Mean	Std	Corr
H-slab	1.83	1.60	0.99	3.04	2.15	0.99	1.83	1.60	0.77	3.04	2.15	0.72
3-slab	2.39	2.22	0.98	5.27	2.45	0.98	2.39	2.22	0.94	5.27	2.45	0.92
W-slab	2.07	2.00	0.99	5.15	1.97	0.99	2.07	2.00	0.92	5.15	1.97	0.95
MI-slab	2.05	2.99	0.98	3.07	2.24	0.98	2.05	2.99	0.93	3.07	2.24	0.90
SI-slab	1.81	1.53	0.99	2.95	1.87	0.98	1.81	1.53	0.84	2.95	1.87	0.63
Global	2.03	2.15	0.98	3.90	2.40	0.98	2.03	2.15	0.92	3.90	2.40	0.88

Mean Average absolute difference between two markers, *Std* Standard deviation of the absolute difference between two markers, *Corr* Correlation coefficient between two markers

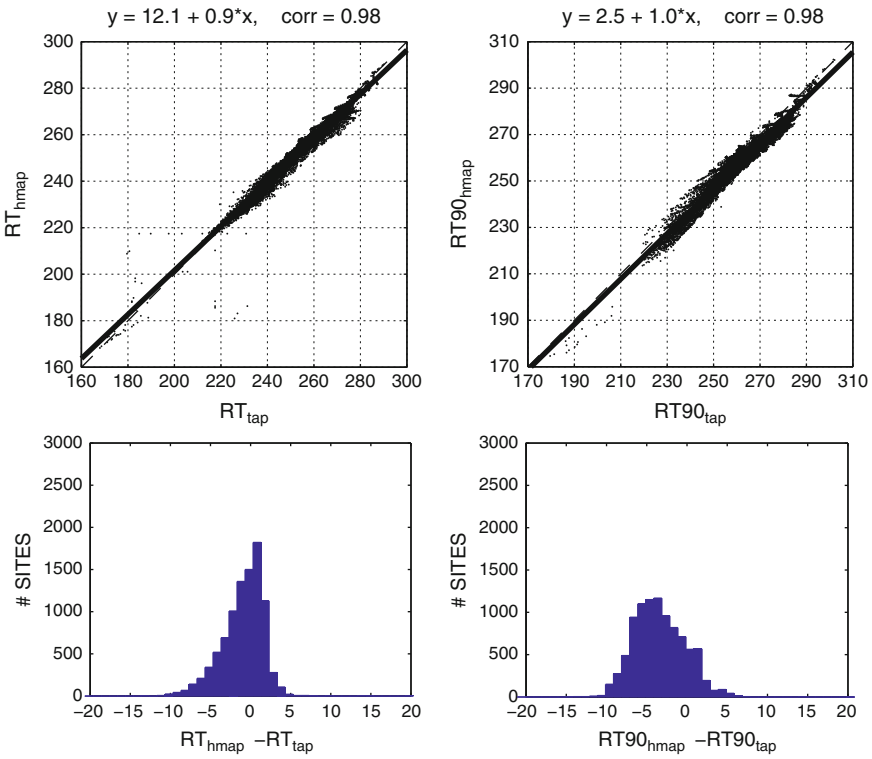

Fig. 2. *Top*: regression lines of RT_{hmap} vs RT_{tap} (*left*) and $\mathrm{RT90}_{hmap}$ vs $\mathrm{RT90}_{tap}$ (*right*), for all 5 slabs of Table 2. *Bottom*: histograms of discrepancies $\mathrm{RT}_{hmap}-\mathrm{RT}_{tap}$ (*left*) and $\mathrm{RT90}_{hmap}-\mathrm{RT90}_{tap}$ (*right*) with 1 ms bins, for all 5 slabs of Table 2

Despite this qualitatively good global performance, the extracellular RT markers do not always yield an accurate estimate of the spatial distribution of TAP-based repolarization time, because some local large discrepancies might ensue. A preliminary study of the reliability of EG-based RT markers has been presented in our recent work [5], here extended to include also the presence of ischemic regions. Nevertheless, HMAP-based markers represent a reliable alternative for estimating RT_{tap} ($\mathrm{RT90}_{tap}$) at recording sites located inside or near the borders of the ischemic region where the classical EG-based markers may fail because of linear ST ramp or absence of T wave.

References

1. Balay, S., et al.: PETSc home page. http://www.mcs.anl.gov/petsc, 2001
2. Colli Franzone, P., Pavarino, L.F.: Math. Mod. Meth. Appl. Sci. **14**(6), 883–911 (2004)

3. Colli Franzone, P., Pavarino, L.F., Taccardi, B.: Math. Biosci. **204**, 132–165 (2006)
4. Colli Franzone, P., Pavarino, L.F., Scacchi, S., Taccardi, B.: Am. J. Physiol. Heart Circ. Physiol. **293**, H2771–H2785 (2007)
5. Colli Franzone, P., Pavarino, L.F., Scacchi, S., Taccardi, B.: FIMH07. In: Sachse, F.B., Seemann, G. (eds.) LNCS, vol. 446, pp. 139–149. Springer, Berlin (2007)
6. Franz, M.R.: Monophasic Action Potentials: Bridging Cells to Bedside. Futura Publishing Company, New York (2000)
7. Luo, C., Rudy, Y.: Circ. Res. **68**(6), 1501–1526 (1991)
8. Nesterenko, V.V., Weissenburger, J., Antzelevitch, C.: J. Cardiovasc. Eletrophysiol. **11**, 948–951 (2000)
9. Pavarino, L.F., Scacchi, S.: SIAM J. Sci. Comp. **31**(1), 420–443 (2008)
10. Poelzing, S., Rosenbaum, D.S.: Am. J. Physiol (Heart Circ. Physiol.) **286**, H2001–H2009 (2004)
11. Punske, B.B., et al.: Ann. Biomed. Engrg. **31**(7), 781–792 (2003)
12. Scacchi, S.: Comp. Meth. Appl. Mech. Engrg. **197**(45–48), 4051–4061 (2008)
13. Viswanathan, P.C., Shaw, R.M., Rudy, Y.: Circulation **99**, 2466–2474 (1999)
14. Yan, G.X., et al.: Circulation **98**, 1921–1927 (1998)